J. Korean Soc. Math. Educ. Ser. B: Pure Appl. Math.
https://doi.org/10.7468/jksmeb.2020.27.1.43
Volume 27, Number 1 (February 2020), Pages 43–50

ISSN(Print) 1226-0657
ISSN(Online) 2287-6081

DOMAIN OF INFLUENCE OF LOCAL VOLATILITY FUNCTION ON THE SOLUTIONS OF THE GENERAL BLACK–SCHOLES EQUATION

Hyundong Kim [a], Sangkwon Kim [a], Hyunsoo Han [b], Hanbyeol Jang [b], Chaeyoung Lee [a] and Junseok Kim [a,*]

Abstract. We investigate the domain of influence of the local volatility function on the solutions of the general Black–Scholes model. First, we generate the sample paths of underlying asset using the Monte Carlo simulation. Next, we define the inner and outer domains to find the effective volatility region. To confirm the effect of the inner domain, we use the root mean square error for the European call option prices, and then change the values of volatility in the proposed domain. The computational experiments confirm that there is an effective region which dominates the option pricing.

1. Introduction

The standard Black–Scholes (BS) partial differential equation [3, 12] assumes constant volatility σ, and the underlying asset S follows the stochastic differential equation

$$\frac{dS}{S} = rdt + \sigma dW_t, \tag{1.1}$$

where t is time, r is the risk-free interest rate, and W_t is a standard Brownian motion. It is well known that the price of European call option $u(S,t)$ is governed by the BS partial differential equation. However, the implied volatility is different for various strike price K in real market [11, 16]. This difficulty is known as the volatility skew and smile [5]. In order to overcome this difficulty, the constant volatility was extended to a local volatility function $\sigma(S,t)$ of the underlying asset and time. Thus,

Received by the editors April 12, 2019. Accepted November 20, 2019.
2010 *Mathematics Subject Classification.* 63N06, 91G80.
Key words and phrases. local volatility function, general Black–Scholes equation, finite difference method.
*Corresponding author.

the price $u(S,t)$ is governed by the following general Black–Scholes model (GBSM) for $(S,t) \in \mathbb{R}^+ \times [0,T)$ [6, 7]:

$$\frac{\partial u(S,t)}{\partial t} = -\frac{\Big(\sigma(S,t)S\Big)^2}{2}\frac{\partial^2 u(S,t)}{\partial S^2} - rS\frac{\partial u(S,t)}{\partial S} + ru(S,t). \tag{1.2}$$

Here, the payoff of European call option $u(S,T)$ has the value $\max(S-K,0)$, where K is strike price and T is maturity date. There are many studies on calibration of local volatility using market data [8]. For example, in [7], Duprie obtained the local volatility function for strike price and maturity using implied volatility. The authors in [1, 4] proposed interesting minimization method. Jackson et al. [10] introduced a method of minimizing the range of the optimization problem in local volatility. In [2], the authors proposed a formulation near expiry of the calibration for the local volatility model using a direct link between implied volatilities and local volatilities. In [8], for European options, the authors developed the calibration of a local volatility surface by applying a second-order Tikhonov regularization. In [15], Turinici calibrated local volatility through a numerical method which applies a Gauss–Newton type approximation of the Hessian and showed a well-executed method in the benchmarks of foreign exchange data. In [9], Glover and Ali constructed a local volatility surfaces using non-parametric two-dimensional regression. They implemented the regression using thin plate splines, the type of radial basis functions, and using Tykhonov regularization and trust-region optimization to find optimal parameter of their proposed local volatility surface.

Although many studies on local volatility have been made, most studies did not consider the effective region of domain for local volatility surface. Therefore, the main goal of this study is to investigate the regional effect of local volatility function on the pricing of the GBSM.

The content of this paper is as follows. In Section 2, we propose the numerical solution algorithm for the GBSM. We perform the numerical experiments in Section 3. Conclusions are drawn in Section 4.

2. Numerical Solution Algorithm

In this section, we propose the numerical solution algorithm by using the fully implicit finite difference scheme and Thomas algorithm. Let $\tau = T - t$ be the time to expiry. Then Eq. (1.2) can be rewritten as the following Cauchy problem for

$(S,\tau) \in \Omega \times (0,T]$:

$$\begin{aligned} \frac{\partial u(S,\tau)}{\partial \tau} &= -\frac{\Big(\sigma(S,\tau)S\Big)^2}{2}\frac{\partial^2 u(S,\tau)}{\partial S^2} - rS\frac{\partial u(S,\tau)}{\partial S} + ru(S,\tau), \\ \frac{\partial^2 u(0,\tau)}{\partial S^2} &= \frac{\partial^2 u(S_{\max},\tau)}{\partial S^2} = 0 \end{aligned} \tag{2.1}$$

with a initial condition $u(S,0) = \max(S-K,0)$ for $S \in \Omega = (0, S_{\max})$, where the infinite domain is truncated to a finite computational domain [13]. Let the number of uniform grid points N_S and N_τ be positive integers. For $1 \le i \le N_S$ and $1 \le n \le N_\tau$, the notations $u(S_i,\tau_n) = u(ih, n\Delta\tau)$ and $\sigma(S_i,\tau_n)$ are simply denoted by u_i^n and σ_i^n, respectively. Here, $h = S_{\max}/N_S$ and $\Delta\tau = T/N_\tau$ are space and time steps, respectively. Now, we discretize Eq. (2.1) by using the fully implicit finite difference scheme:

$$\frac{u_i^{n+1}-u_i^n}{\Delta\tau} = \frac{(\sigma_i^{n+1}S_i)^2}{2}\frac{u_{i-1}^{n+1}-2u_i^{n+1}+u_{i+1}^{n+1}}{h^2} + rS_i\frac{u_{i+1}^{n+1}-u_{i-1}^{n+1}}{2h} - ru_i^{n+1}. \tag{2.2}$$

Let $\alpha_i = \dfrac{rS_i}{2h} - \dfrac{(\sigma_i^{n+1}S_i)^2}{2h^2}$, $\beta_i = \dfrac{1}{\Delta\tau} + \dfrac{(\sigma_i^{n+1}S_i)^2}{h^2} + r$, $\gamma_i = -\dfrac{rS_i}{2h} - \dfrac{(\sigma_i^{n+1}S_i)^2}{2h^2}$, $b_i = \dfrac{u_i^n}{\Delta\tau}$. Then, we can rewrite Eq. (2.2) as follows:

$$\alpha_i u_{i-1}^{n+1} + \beta_i u_i^{n+1} + \gamma_i u_{i+1}^{n+1} = b_i. \tag{2.3}$$

For the boundary condition, we use the linear boundary condition at S_0 and S_{N_S}. That is, $u_0^n = 2u_1^n - u_2^n$ and $u_{N_{S+1}}^n = 2u_{N_S}^n - u_{N_{S-1}}^n$ for all n [17]. To solve the discrete Eq. (2.3), we apply the Thomas algorithm [14].

3. Numerical Experiments

In this section, we implement the numerical experiments. In all numerical experiments, unless otherwise noted, we perform Monte Carlo simulations with 1.0E+5 samples and we use the maturity date $T = 1$, temporal step size $\Delta t = 1/365$, risk-free interest rate $r = 0.015$, and strike prices $(K_1, K_2, K_3, K_4, K_5) = (80, 90, 100, 110, 120)$. All computations are done using MATLAB R2018. To generate the sample paths of underlying asset, we shall configure the two-step as follows. First, we take the natural logarithm on the both sides of Eq. (1.1) and then apply the *Itô*'s lemma. Then, we can obtain the following well-known decision process of asset value with respect to the standard normal distribution Z:

$$S(t) = S(0)\exp\Big((r - \frac{\sigma^2}{2})t + \sigma\sqrt{t}Z\Big), \tag{3.1}$$

which follows the log-normal distribution with mean $(r - \frac{\sigma^2}{2})t$ and variance $\sigma^2 t$. Also, we discretize Eq. (3.1) into the following equation:

$$S(t+\Delta t) = S(t)\exp\Big((r - \frac{\sigma^2}{2})\Delta t + \sigma\sqrt{\Delta t}Z\Big), \tag{3.2}$$

Next, let us consider the computational domain $\Omega = (0, S_{\max}) \times (0, T]$. By using the Monte Carlo simulation and Eq. (3.2) with $\sigma = 0.25$, $r = 0.015$, $\Delta t = 1/365$, we generate random sample paths of underlying asset. Let $\Omega_{\text{in}} = \Big\{(S, t_m) : S_k^m(\lfloor k\frac{\alpha}{100}\rfloor) \le S \le S_k^m(\lfloor k(1-\frac{\alpha}{100})\rfloor)\Big\}$ be the inner domain, where $\lfloor\cdot\rfloor$ is a floor function, S_k^m is a matrix of all simulated S and is generated at time t in ascending order, k is the number of simulations and $m = t/\Delta t$, $1 \le m \le N_t$ where N_t is the number of uniform grid points. Above condition means that $S_k^m(\lfloor k\frac{\alpha}{100}\rfloor)$ and $S_k^m(\lfloor k(1-\frac{\alpha}{100})\rfloor)$ are underlying asset prices on the maximum value among the values of the lower $\alpha\%$, and on the minimum value among the upper $\alpha\%$ values at time t, respectively. In detail, using $\Big(\lfloor k\frac{\alpha}{100}\rfloor\Big)$-th and $\Big(\lfloor k(1-\frac{\alpha}{100})\rfloor\Big)$-th indices, we define Ω_{in} such as grayscale shadow sketched in Fig 1. Let Ω_{out}=Ω_{in}^c be the outer domain. From now on, to observe the influence of inner domain Ω_{in}, we define

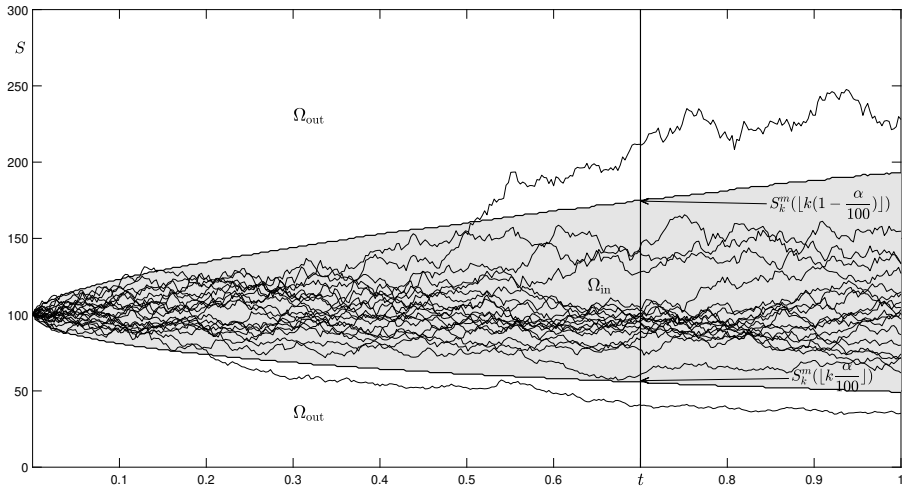

Figure 1. Generating sample paths, and setting of $S_k^m(\lfloor k\frac{\alpha}{100}\rfloor)$, $S_k^m(\lfloor k(1-\frac{\alpha}{100})\rfloor)$, Ω_{in}, and Ω_{out}.

the reference solution $V_j^{ref} = V^{ref}(S_0, K_j)$ and numerical solution $V_j = V(S_0, K_j)$ which are priced by the GBSM for each strike price K_j, $1 \le j \le 5$. In this test, the

reference solution V_j^{ref} is the European call option price when the underlying asset price $S_0 = 100$, $\sigma_1 = \sigma_2 = 0.25$ and K_j for all j. Furthermore, we define the local volatility function as follows:

$$\sigma(S,t;\sigma_1,\sigma_2) = \begin{cases} \sigma_1 & \text{if (S, } t) \in \Omega_{\text{in}}, \\ \sigma_2 & \text{if (S, } t) \in \Omega_{\text{out}}. \end{cases}$$

In Fig. 2, we can see the schematics of inner domain Ω_{in} and of outer domain Ω_{out} with corresponding volatilities σ_1 and σ_2.

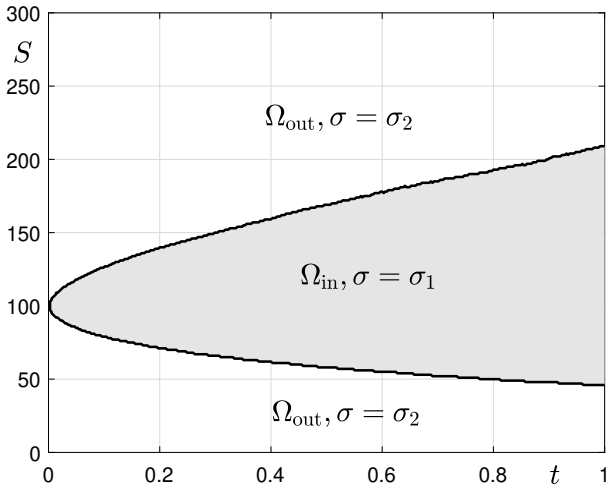

Figure 2. Inner domain Ω_{in} and outer domain Ω_{out} with corresponding volatilities σ_1 and σ_2.

In Fig. 3, for $0 \leq S \leq S_{max}$, $V(S, K_3)$ is calculated with $\sigma_1 = 0.25$, $\sigma_2 = 0.35$ and then is compared with $V^{ref}(S, K_3)$. The result in Fig. 3 shows that $V(S, K_3)$ and $V^{ref}(S, K_3)$ are not significantly different.

Now, we use the root mean square error (RMSE) to confirm the effect of the inner domain Ω_{in}, which is defined by

$$RMSE = \sqrt{\frac{1}{N}\sum_{j=1}^{N}(V_j^{ref} - V_j)^2},$$

In Ω_{in} and Ω_{out}, we investigate the RMSE while changing the volatility σ_1 or σ_2 from 0 to 0.5. First, we fixed $\sigma_2 = 0.25$ in Ω_{out} and calculated V_j with various σ_1 values from 0 to 0.5 in Ω_{in} (circle marker). On the other hand, we fixed $\sigma_1 = 0.25$ in Ω_{in} and calculated V_j with various σ_2 values from 0 to 0.5 in Ω_{out} (square marker). Fig. 4(a), (b), (c), and (d) show the RMSEs for $\alpha = 1, 5, 10, 15$, respectively. The

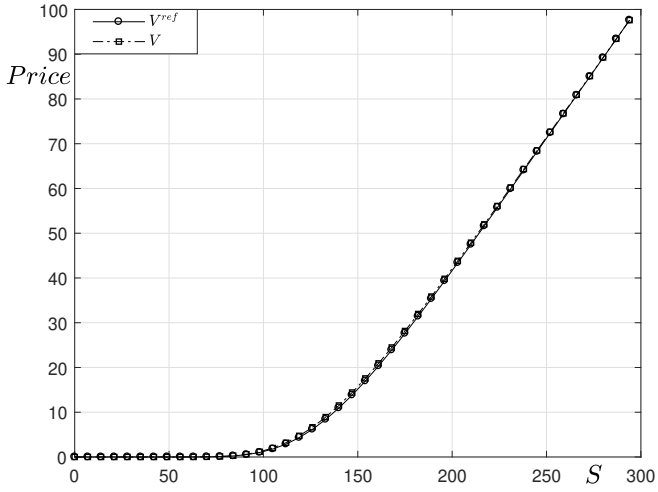

Figure 3. Call option price.

results in Fig. 4 show that RMSEs are relatively small when changing σ_2 in Ω_{out} than when changing σ_1 in region Ω_{in}. Ultimately, this means that the influence of Ω_{in} is greater than the influence of Ω_{out} when calculating the option price.

4. Conclusions

This paper focuses on the volatility region that affects the option price. To discover of influence on the generated volatility region, we performed the numerical experiments using the RMSE. To find the numerical solution for the GBSM, we used the fully implicit finite difference scheme and applied the Thomas algorithm. The Monte Carlo simulation and the decision process of asset price were used to generate the sample paths of underlying asset and the influential volatility region. In the numerical experiments, we proposed the inner and outer domains to investigate the influential volatility region. The computational results show that there is no big difference between the option prices obtained using the separated volatility region and the constant volatility. In a more complex situation, we have found that the results of numerical test using the RMSE are smaller when changed the volatility in outer domain than when we changed the volatility in inner domain. As a consequence, the proposed inner domain becomes the influential volatility region. These results provide important information to the reconstruction of local volatility function. Using these results, in the future work for local volatility study, we

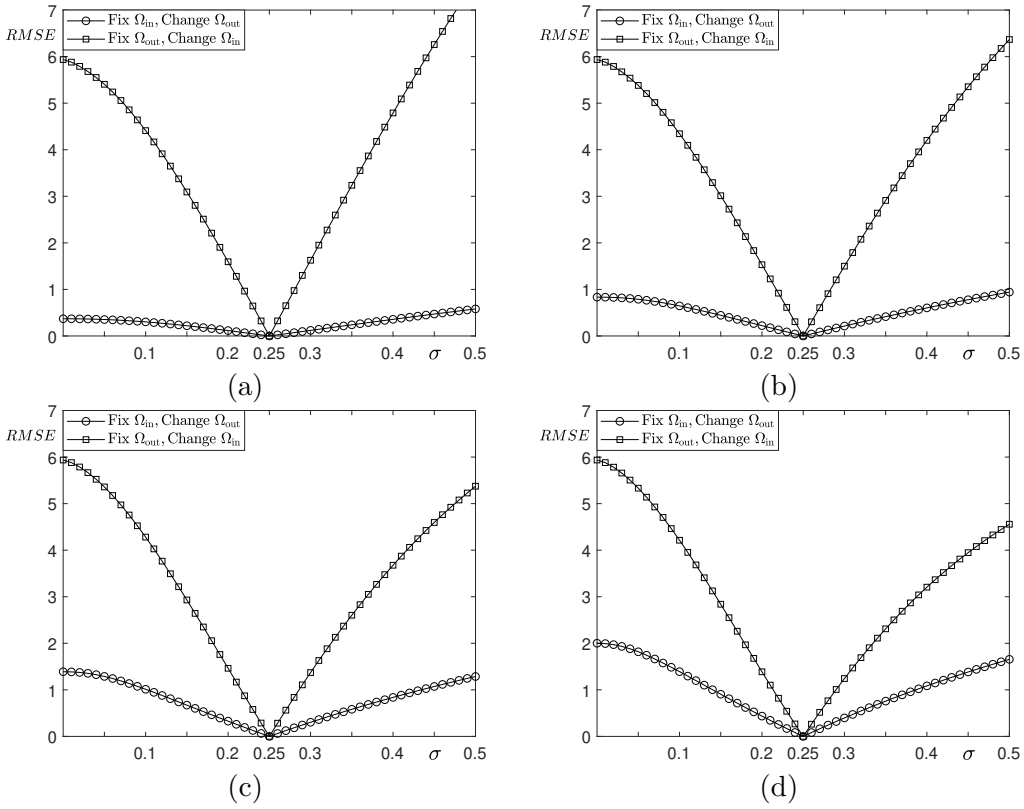

Figure 4. (a), (b), (c), and (d) are the RMSEs for $\alpha = 1, 5, 10, 15$, respectively.

will investigate a specific region rather than whole domain to find local volatility function.

Acknowledgment

The corresponding author (J.S. Kim) expresses thanks for the support from the BK21 PLUS program.

References

1. M. Avellaneda, C. Friedman, R. Holmes & D. Samperi: Calibrating volatility surfaces via relative-entropy minimization. Appl. B Math. Finance **4** (1997), 37-64.
2. H. Berestycki, J. Busca & I. Florent: Asymptotics and calibration of local volatility models. Quant. Finance **2** (2002), 61-69.

3. F. Black & M. Scholes: The pricing of options and corporate liabilities. J. Polit. Econ. **81** (1973), 637-654.
4. J.N. Bodurtha & M. Jermakyan: Nonparametric estimation of an implied volatility surface. J. Comput. Finance **2** (1999), 29-60.
5. S. Chen, Z. Zhou & S. Li: An efficient estimate and forecast of the implied volatility surface: A nonlinear Kalman filter approach. Econ. Model. **58** (2016), 655-664.
6. E. Derman & I. Kani: Riding on a smile. Risk Magazine **7** (1994), 32-39.
7. B. Dupire: Pricing with a smile. Risk Magazine **7** (1994), 18-20.
8. J. Geng, I.M. Navon & X. Chen: Non-parametric calibration of the local volatility surface for European options using a second-order Tikhonov regularization. Quant. Finance **14** (2014), 73-85.
9. J. Glover & M.M. Ali: Using radial basis functions to construct local volatility surfaces. Appl. Math. Comput. **217** (2011), 4834-4839.
10. N. Jackson, E. Süli & S. Howison: Computation of deterministic volatility surfaces. J. Comput. Finance **2** (1999), 5-32.
11. J. Liang & Y. Gao: Calibration of implied volatility for the exchange rate for the Chinese Yuan from its derivatives. Econ. Model. **29** (2012), 1278-1285.
12. R.C. Merton: Theory of rational option pricing. Bell J. Econ. Manag. Sci. **4** (1973), 141-183.
13. D. Tavella & C. Randall: Pricing financial instruments: The finite difference method. Wiley, New York, 2000.
14. L. Thomas: Elliptic problems in linear differential equations over a network: Watson scientific computing laboratory. Columbia University, New York, 1949.
15. G. Turinici: Calibration of local volatility using the local and implied instantaneous variance. J. Comput. Finance **13** (2009), 1-18.
16. J. Wang, S. Chen, Q. Tao & T. Zhang: Modelling the implied volatility surface based on Shanghai 50ETF options. Econ. Model. **64** (2017), 295-301.
17. H. Windcliff, P.A. Forsyth & K.R. Vetzal: Analysis of the stability of the linear boundary condition for the Black–Scholes equation. J. Comput. Finance **8** (2004), 65-92.

[a]DEPARTMENT OF MATHEMATICS, KOREA UNIVERSITY, SEOUL 02841, REPUBLIC OF KOREA
Email address: rlagusehd@korea.ac.kr; *cfdkim@korea.ac.kr

[b]DEPARTMENT OF FINANCIAL ENGINEERING, KOREA UNIVERSITY, SEOUL 02841, REPUBLIC OF KOREA